



Contents lists available at ScienceDirect

Arabian Journal of Chemistry

journal homepage: www.ksu.edu.sa

Insights into the photocatalytic role of glycine-assisted sol-gel auto-combustion synthesized (Co, Mn)(Co, Mn)₂O₄ nanostructures for efficient visible light-driven degradation of methyl orange

Ghazal Oroumi^a, Foroozan Samimi^a, Makarim A. Mahdi^b, Elmuez A. Dawi^c, Masoud Salavati-Niasari^{a,*}

^a Institute of Nano Science and Nano Technology, University of Kashan, Kashan P. O. Box. 87317-51167, Iran

^b Department of Chemistry, College of Education, University of Al-Qadisiyah, Diwaniyah, Iraq

^c Nonlinear Dynamic Research Center (NDRC), College of Humanities and Sciences, Ajman University, P.O. Box 346 Ajman, United Arab Emirates

ARTICLE INFO

Keywords:

Cobalt-Manganese Oxides Spinel Nanostructures
Methyl Orange
Photodegradation Efficiency

ABSTRACT

Research on the use of new materials and the improvement of existing fast ways for removal of water pollutants is still challenging. This work documented rational fabrication of (Co, Mn)(Co, Mn)₂O₄ nanoparticles as nano-photocatalyst materials with improved charge carrier separation and strong redox potential for efficient degradation of methyl orange (MO) in wastewater. This investigation illustrated that the Co/Mn molar ratio can greatly affect the textural and structural properties. From the point of view of size and shape, the optimum product with 1:3 M ratio of Co to Mn precursors was selected as a catalyst in the photocatalysis process. The prepared highly crystallized phase of tetragonal (Co, Mn)(Co, Mn)₂O₄ describe an optical band gap of 1.7 eV, according to the DRS data, which make them as efficient visible driven photocatalysts. The photodegradation experiments of spinel mixed structures were assessed by investigation of photocatalyst dosages and initial MO concentrations to unravel how these operational parameters affect Co-Mn-O photocatalysis. A remarkable discoloration capability of 68.07 % could result from the catalyst dosage of 0.04 g and dye concentration of 15 mg/L after 120 min of visible light. The kinetics survey further unveiled the maximum rate constant of 0.0080 min⁻¹ for the MO degradation. In the scavenger trials, singlet oxygen (¹O₂) and superoxide ([•]O₂⁻) radicals were principal reactive oxygen species (ROS) responsible for pollutant photodegradation in the presence of pure (Co, Mn)(Co, Mn)₂O₄ structures. In addition, the cyclic performance of catalyst depicted a removal efficiency of 60.1 % over 5 runs.

1. Introduction

Access to water has been the major issue for the creatures of the planet (Yaqoob et al., 2020). Humans have always looked for additional sources of water. Nowadays, the reduction of fresh and potable water resources has involved people in many troubles (Aslam et al., 2019a; Joseph et al., 2019; Rahimi-Nasrabadi et al., 2019). Dyes are known as persistent organic compounds in textiles, cosmetics, plastics, etc, so they have coloring and binding ability on the surface of substrates through several approaches like physisorption, covalent bonds and generation of metal ions/salt-based metal complexes (Behvandi et al., 2020; Bonthula et al., 2023; Hosny et al., 2023; Taifi et al., 2022). Therefore, because of their stability and their resistance to biodegradability, it is necessary to

decrease potential hazards of dyes to agricultural production, aquatic organisms, and human health. As a monoazo dye, methyl orange (MO) with sulfur group and aromaticity can result in harmful diseases such as eye irritation and skin problems (Onwudiwe et al., 2023). In the meantime, researchers, along with technologists, have paid special attention to achieve various methods to prevent water wastage, and treat polluted water (Hasan and Muhammad, 2020; Shanmugam et al., 2019). Through the years, several initiatives have been taken to incorporate a variety of wastewater treatment technologies, including conventional filtration, coagulation-flocculation, and biological treatment systems (Marsooli et al., 2020; Obotey Ezugbe and Rathilal, 2020; Mahdi et al., 2021; Aljeboree et al., 2021; Ganduh et al., 2021). In order to execute the photocatalysis process, the catalyst material must possess

* Corresponding author.

E-mail address: salavati@kashanu.ac.ir (M. Salavati-Niasari).

<https://doi.org/10.1016/j.arabjc.2023.105588>

Received 23 June 2023; Accepted 24 December 2023

Available online 27 December 2023

1878-5352/© 2023 The Author(s). Published by Elsevier B.V. on behalf of King Saud University. This is an open access article under the CC BY-NC-ND license (<http://creativecommons.org/licenses/by-nc-nd/4.0/>).

the capacity to be stimulated by visible or ultraviolet light (Amin Marsooli et al., 2020; Naik et al., 2023). In fact, the ability to generate electron-holes is the primary stage of photocatalysis. When semiconductor materials are exposed to UV or visible light, they can initiate a range of reactions in aqueous environments, resulting in the eradication of pollutants from water (Al-Mamun et al., 2019; Badvi and Javanbakht, 2021; Jabbar and Graimed, 2022). The semiconductors used in the photocatalytic process include a wide range of materials (Bloise et al., 2009; Rostami et al., 2021). Nanotechnology has enabled researchers to use nanomaterials in a variety of water and wastewater treatment technologies (Aslam et al., 2019b; Taghipour et al., 2019). Nanomaterials can be utilized to optimize water treatment processes, including membrane and filtration, precipitation and, notably, photocatalysis (Ahmad et al., 2022; Aragaw et al., 2021; Ren et al., 2021). Transition metal oxides in different structures are one of the great families of semiconductors (Karthikeyan et al., 2020; Wang et al., 2020). Cobalt manganese based-spinel oxides namely $MnCo_2O_4$ and $CoMn_2O_4$ introduce unique electrical features and multiple oxidation states, which play a vital role in photocatalytic domain (Kihal et al., 2024; Mkhaliid et al., 2023). However, owing to high recombination of photogenerated charge carrier, the photodegradation efficiency of these compositions is still not up to expectations. As a $Mn_xCo_{3-x}O_4$ bimetallic oxide with $x = 1.5$, $(Co, Mn)(Co, Mn)_2O_4$, has drawn the focus of many researchers due to its low cost, availability, stability, and metal centers with redox-activity, making it a useful heterogeneous catalyst and battery anode material (Yu, L. et al., 2013; Zhao et al., 2014). Numerous ways have been documented for the production of $(Co, Mn)(Co, Mn)_2O_4$, including the ball mill (Masi et al., 2016), precipitation (Tang et al., 2017), coprecipitation, and sol-gel (Liang et al., 1998). In this project, we propose a novel and facile programmable process for the synthesis spinel-type binary transition metal oxides, namely $(Co, Mn)(Co, Mn)_2O_4$ nanostructures in the presence of glycine as both fuel and structure-directing agent. More encouragingly, the impact of the (Co, Mn) precursor ratio on the compositional and structural superiority was deeply evaluated. Based on the literature review, this project aims to investigate less studied applications of these materials, including photocatalytic activity. The photocatalysis performances of optimized Co-Mn-O

nanostructures were systematically investigated through diverse operational parameters including effect of dye concentration, and catalyst dosage in the degradation of MO dye under visible light. The possible photocatalytic mechanism of the products was discussed based on experimental results.

2. Experimental

2.1. Materials

All of the chemical components used in this study including cobalt (II) nitrate hexahydrate ($Co(NO_3)_2 \cdot 6H_2O$), manganese(II) nitrate tetrahydrate ($Mn(NO_3)_2 \cdot 4H_2O$), glycine ($C_2H_5NO_2$) and tetraethylenepentamine (TEPA), ethylenediaminetetraacetic acid (EDTA), benzoic acid (BA), 1,4-Benzoquinone (BQ) and sodium azide (NaN_3), were obtained from Merck Company (Darmstadt, Germany) and applied without any purification. In addition, MO ($C_{14}H_{14}N_3NaO_3S$) employed as a contaminant, was obtained from Aldrich (Chemical Co., Milwaukee, WI, USA).

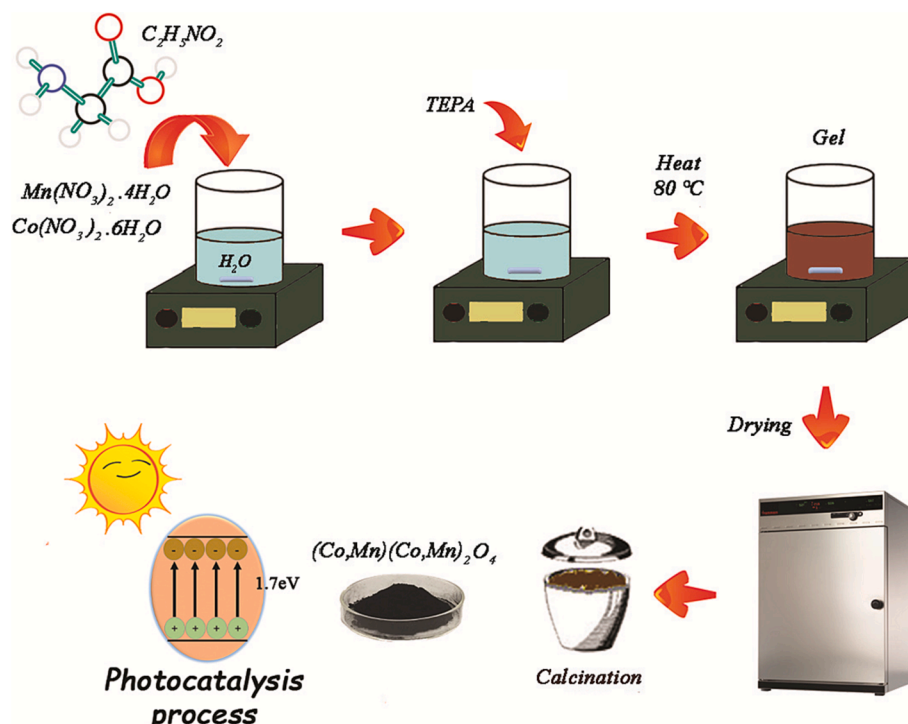
2.2. Characterization of $(Co, Mn)(Co, Mn)_2O_4$ nanostructures

2.2.1. X-ray diffraction (XRD)

The type of structure and the purity of the as-synthesized nanoparticles were confirmed by collecting XRD patterns with a diffractometer of the Philips company with X'PertPro monochromatized $Cu K\alpha$ radiation ($\lambda = 1.54 \text{ \AA}$), in the 2θ values between 10 and 80 with the step size of 0.05° . To analyze the acquired data for different samples, PANalytical HighScore Plus software was applied. By applying the Scherrer equation (Holzwarth and Gibson, 2011):

$$D_c = K\lambda/\beta\cos\theta \quad (1)$$

where β is the width of the observed diffraction peak at its half maximum intensity (FWHM), K is the shape factor, which takes a value of about 0.9, and λ is the X-ray wavelength ($CuK\alpha$ radiation, equals to 0.154 nm), the size of the crystallites for samples can be estimated.



Scheme 1. Schematic model of the formation for auto-combustion synthesized $(Co, Mn)(Co, Mn)_2O_4$ nanoparticles in the presence of glycine as fuel.

Table 1
Preparation conditions of Mn-Co spinel oxides.

No.	Co: Mn ratio	Co: Glycine ratio	Phase purity	Average Crystallite size/XRD (nm)	Average Particle Size/SEM (nm)
1	2:3	1:2	(Co, Mn)(Co, Mn) ₂ O ₄ / MnO ₂	31.5	84.63
2	1:3	1:3	(Co, Mn)(Co, Mn) ₂ O ₄	30	74.11
3	3:3	1:3	(Co, Mn)(Co, Mn) ₂ O ₄ / MnCo ₂ O ₄	20	88.49

2.2.1.1. Fourier-transform infrared (FT-IR) spectroscopy. For FT-IR analysis, a spectrophotometer (Shimadzu Varian 4300) was employed for studying the functional group composition of as-fabricated cobalt–manganese oxide spinel nanostructures in the range between 400 and 4000 cm⁻¹ (Nicolet Magna-IR 550, Potassium bromide (KBr) pellets) at 4 cm⁻¹ resolution. For this process, the sample were obtained by a mixture form 5 mg of (Co,Mn)(Co,Mn)₂O₄ and 95 mg of KBr and grounding by an agate mortar and subsequently pressing under a pressure of 2 tons with a pelletizer. Then, the resulting pellet was placed in the path of the IR beam.

2.2.1.2. Field emission scanning electron microscopy (FE-SEM) and energy dispersive X-ray (EDS) studies. An examination of the morphology and distribution of nanoparticles was conducted via FE-SEM (Sigma 300 Zeiss) using the secondary electron (SE) detector and an accelerating voltage of 10.0 kV. To support better imaging quality, samples for FE-SEM studies were covered by a 5-nm thick gold layer. EDS instrument was utilized to characterize the elemental constituents and purity of synthesized samples with 20 kV stimulating charge.

2.2.1.3. Transmission electron microscopy (TEM). Additional morphological features for optimum samples were recorded by TEM measurement (Philips EM208) with an accelerating voltage of 200 kV.

2.2.1.4. Vibrating sample magnetometer (VSM). The magnetic properties of the synthesized nanoparticles were studied using a magnetometer device produced by Meghnatis Daghigh Kavir Company from Iran.

2.2.1.5. Diffuse reflectance spectroscopy (DRS). The UV–vis diffuse reflectance analysis was executed by utilizing a UV–vis spectrophotometer (Shimadzu, UV2550, Japan). The optical bandgap energy of (Co,Mn)(Co,Mn)₂O₄ semiconductor can be obtained from Tauc method by the following:

$$(ah\nu)^n = A(h\nu - B.G.) \quad (2)$$

where light frequency, Planck constant, absorbance, material constant, and optical bandgap are referred to as ν , h , A , and B.G., respectively.

2.3. Synthesis of mixed spinel structure (Co,Mn)(Co,Mn)₂O₄ nanomaterial

For the synthesis of (Co, Mn)(Co, Mn)₂O₄ via simple sol–gel auto-combustion method, 1.0 g of Co(NO₃)₂·6H₂O was dissolved in 10 mL of deionized water. Next, 2.05 g of Mn(NO₃)₂·4H₂O was combined into the above mixture. Then, nitrate solution with 3:1 M ratio of Mn:Co was mixed using a magnetic stirrer for 5 min. After that, 0.82 g of glycine as an amino acid was slowly added to the container containing the metal ions. TEPA was used to adjust the pH of the medium to 10. The temperature of hot plate was set at 80 °C with continuous stirring (800 rpm). After 90 min, a red gel was obtained. The resulting gel was transferred to

an oven to drying process. The dried gel was first placed in an air furnace at 450 °C for 3 h. The obtained powder underwent a temperature of 750 °C for duration of 5 h in the following step (Scheme 1). In Table 1, stoichiometric ratios and method information have been reported.

2.4. Photocatalysis process

0.04 g of the optimal samples was combined with 40 mL of the dye solution, having different concentrations of 5, 10, 15 and 20 mg/L (pH = 7), to initiate the photocatalysis process. The photocatalysis process began with the aeration of the solution for duration of 20 min. Following aeration, a sample was taken and then the sample container was exposed to visible light (20 cm away). During reaction, an Osram 400 W visible light (containing a wavelength in the range of 400 to 780 nm) was employed. Sampling was performed at 10 min intervals; however, initial sampling was performed after 20 min. All portions of the photocatalysis process were executed without external light and at ambient temperature. The absorbance was documented by means of a UV–Visible spectrophotometer in order to evaluate the discoloration of the dyes. The following formula was used to calculate the discoloration percentage:

$$\%Discoloration = (A_0 - A_t)/A_0 \times 100 \quad (3)$$

Where A_0 and A_t are the absorbance values of the dye solution at 0 and t min, respectively.

3. Result and discussion

3.1. Crystal structure

The crystal structure and formation of the intended structure of the synthesized samples were determined through X-ray diffraction analysis. Fig. 1 compares the resulting XRD patterns of mixed manganese cobalt oxides with a spinel structure synthesized at diverse conditions. As seen in Fig. 1(a-c), the (Co, Mn)(Co, Mn)₂O₄ structures (JCPDS PDF Card No. 00–018-0408) were formed as main phase for three different samples. Based on previous reported literatures (Lin et al., 2021; Lu et al., 2023), the presence of the (Co, Mn)(Co, Mn)₂O₄ phase is confirmed by the diffraction signals at $2\theta = 18.2^\circ, 29.3^\circ, 31.3^\circ, 32.8^\circ, 36.4^\circ, 38.7^\circ, 44.8^\circ, 50.5^\circ, 51.5^\circ, 54.4^\circ, 56.6^\circ, 59.0^\circ, 60.5^\circ, 65.1^\circ, \text{ and } 74.8^\circ$ assigned to the (1 1 1), (2 0 2), (2 2 0), (1 1 3), (3 1 1), (0 0 4), (4 0 0), (2 2 4), (3 3 2), (2 0 5), (3 3 3), (5 1 1), (4 0 4), (4 4 0), and (5 3 3) planes, respectively. Noticeably, it could be observed that the molar ratio of Co and Mn precursors can effectively govern the phase purity and crystallographic information of the products. As shown in Fig. 1a, the XRD pattern confirms mixed crystal structures of the (Co, Mn)(Co, Mn)₂O₄ and MnO₂ by adjusting the Co:Mn molar ratio of 2:3 in the precursor mixture. In sample No. 1, the corresponding reflection (1 1 0) of MnO₂ (JCPDS PDF Card No. 00–050-0866) can be detected at 28.8°. However, when the molar ratio of Co to Mn reduced from 2:2 : 33 to 1] : 3:3 within the mixture, highly crystallized phase of tetragonal (Co, Mn)(Co, Mn)₂O₄ was obtained without other impurities (Fig. 1b). Whereas, under the same reaction conditions of Co/Mn molar ratio (Fig. 1c), the diffraction peaks in the XRD pattern of samples can be indexed to the two phases of the (Co, Mn)(Co, Mn)₂O₄ and MnCo₂O₄ (JCPDS PDF Card No. 00–023-1237). In general, the XRD results showed that calcination at 750 °C helps increase the crystallinity of the desired compound. Furthermore, using the data collected from XRD analysis and using the Scherrer equation (Holzwarth and Gibson, 2011), the size of the crystallites for samples No. 1, 2, and 3 was calculated to be near 31.5, 30, and 20 nm, respectively.

3.2. Bond structure

A deeper understanding of the functional groups of organic compounds can be gained through FT-IR analysis. The FT-IR spectrum of the as-synthesized (Co, Mn)(Co, Mn)₂O₄ is illustrated in Figure S1. The absorption peaks at 3432 and 1640 cm⁻¹ are related to the stretching and bending vibrational absorptions of O–H, respectively (Monsef and Salavati-Niasari, 2023). The peaks at 505 and 619 cm⁻¹ corresponded to

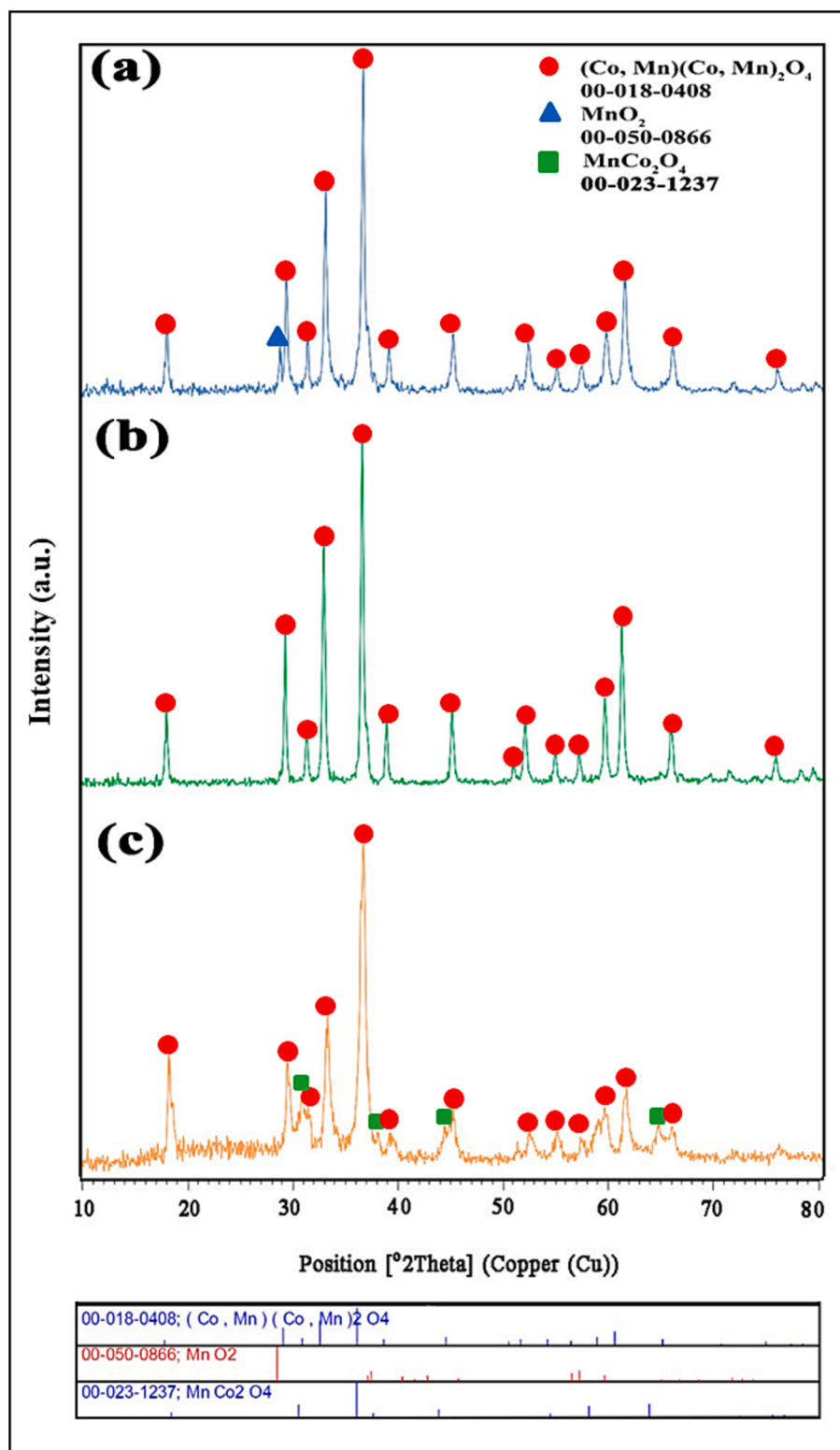


Fig. 1. XRD patterns of Mn-Co spinel oxides synthesized in the different ratios of precursors (Co: Mn) (a) 2:3, (b) 1:3, and (c) 3:3.

the stretching vibration of Co-O and Mn-O, respectively (Topka et al., 2021). Furthermore, an EDS analysis was implemented to guarantee the quality of the synthesized particles. The results of the EDS analysis are shown in Figure S2(a-c). As seen, EDS analyses confirms Co, Mn and O elements. The Au peak is observed in the EDS spectra because of the coating of the sample before SEM analysis.

3.3. Morphology studies

Considering that different conditions used in the synthesis of nanoparticles, SEM analysis was employed to check the morphology of the products. Fig. 2(a-i) shows the SEM images and particle size distribution plots obtained from samples No. 1, 2 and 3 in two magnifications. As it is clear from the images, the particles in all three samples are spherical, although this was predictable because of the use of glycine in all three samples. In sample No. 2 (Fig. 2 (d, e)), the particles are monodispersed

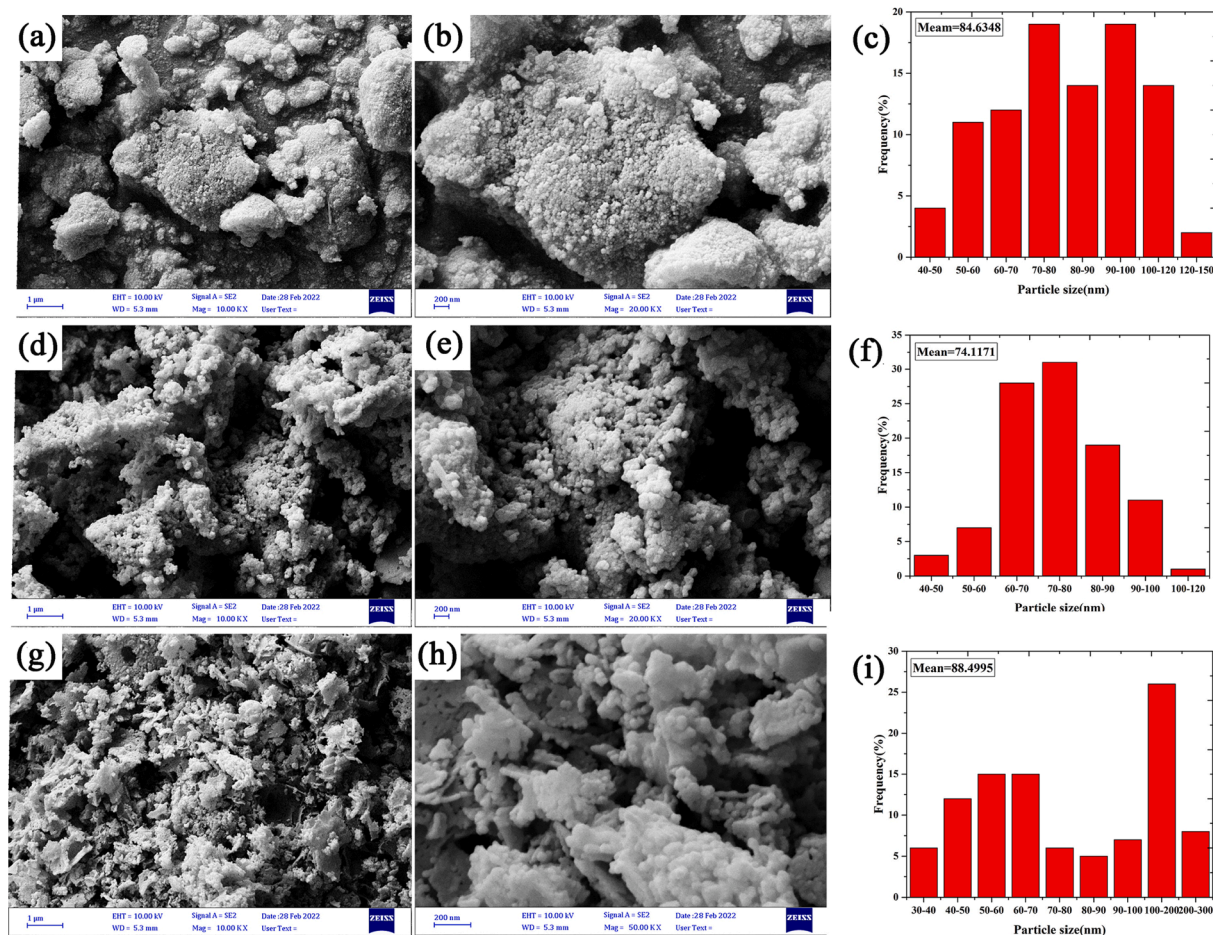


Fig. 2. FE-SEM micrographs and particle size distribution histograms of Mn-Co spinel oxides synthesized in the different ratios of precursors (Co: Mn) (a-c) 2:3, (d-f) 1:3, and (g-i) 3:3.

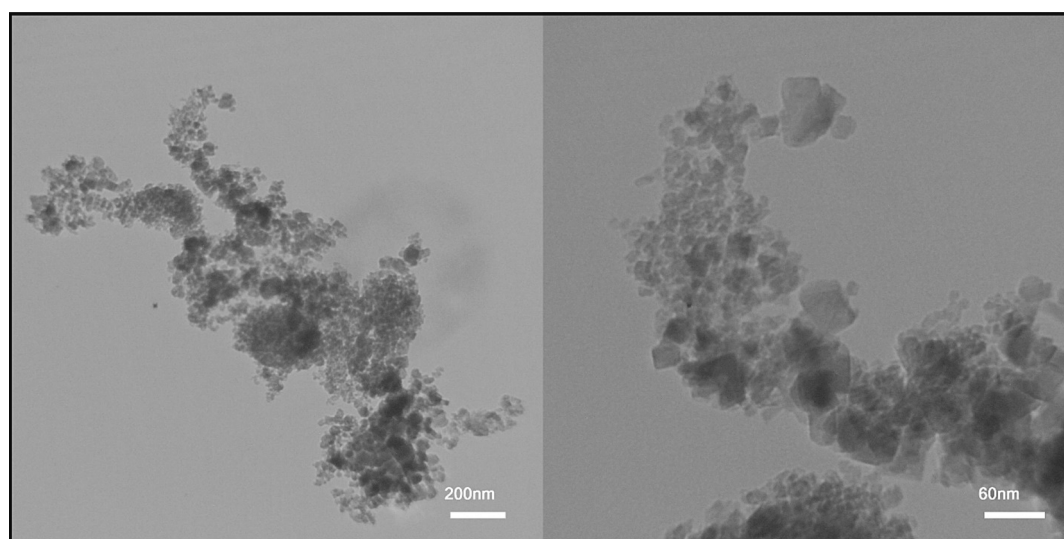


Fig. 3. TEM images of the (Co, Mn)(Co, Mn)₂O₄ nanoparticles (sample No. 2).

and smaller than the other two samples. The reason for this occurrence can be attributed to the using the optimum amounts of glycine and metal precursors during the reaction. In samples No. 1 (Fig. 2 (a, b)) and 3 (Fig. 2 (g, h)), according to the images, the particles adhere together and are agglomerated. By examining the results of XRD and SEM analyses

and the importance of particle size and morphology, sample No. 2 was selected as the optimal sample and other analyses were applied for this sample. The form of the particles was investigated in depth using TEM images. TEM images obtained from (Co, Mn)(Co, Mn)₂O₄ nanoparticles (sample No. 2) are shown in Fig. 3. The images revealed that the

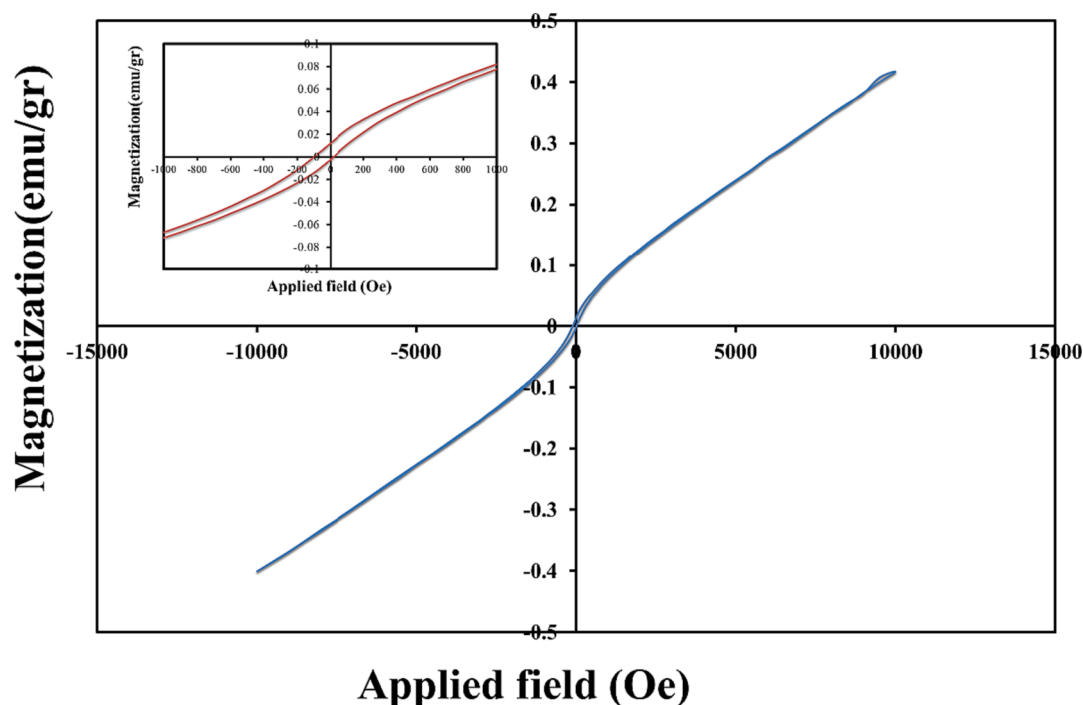
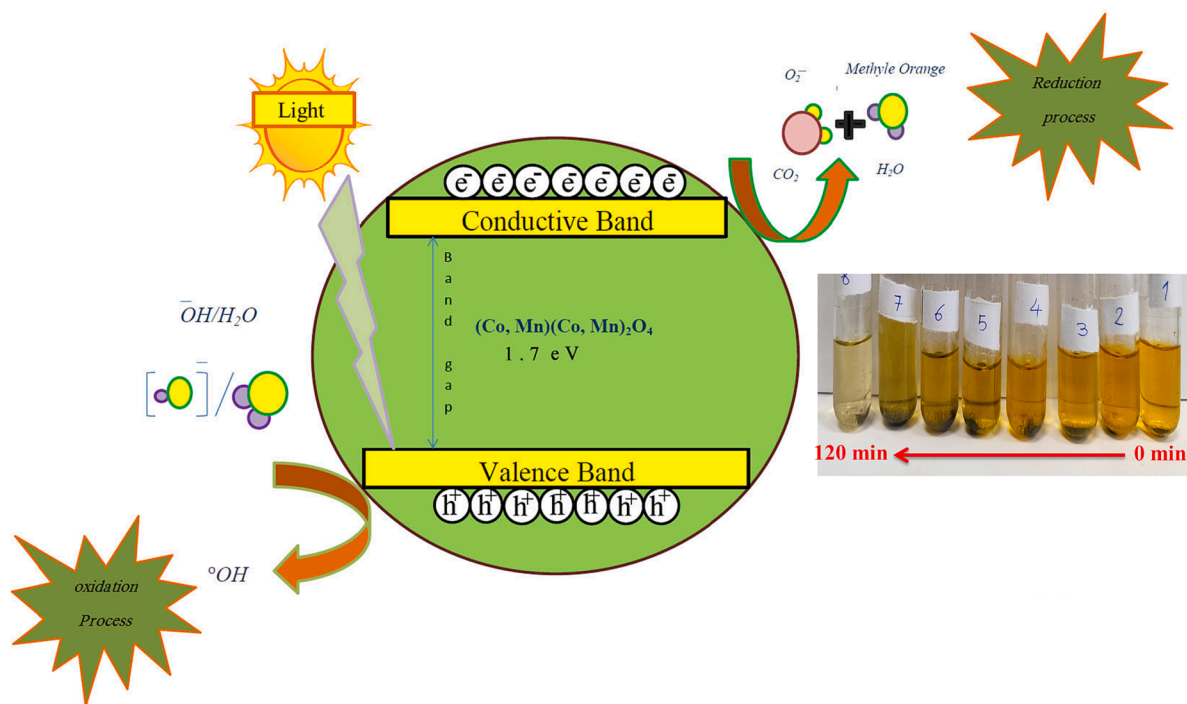


Fig. 4. Magnetization versus applied magnetic field at room temperature (inset shows the magnified hysteresis loop) of the (Co, Mn)(Co, Mn)₂O₄ nanoparticles (sample No. 2).



Scheme 2. Schematic of charge transfer mechanism in (Co, Mn)(Co, Mn)₂O₄ nanoparticles under visible region.

nanoparticles were sticking together and agglomerated.

3.4. Magnetic properties

The magnetic properties of nanomaterials, which can be understood through the use of VSM analysis, can be a valuable element in the study of photocatalytic virtues. The magnetic properties of catalysts can help in their better collection. The magnetization evaluation as a function of the applied field of the (Co, Mn)(Co, Mn)₂O₄ nanoparticles (sample No. 2) was discussed at 300 K and is shown in Fig. 4. The hysteresis loop with

the coercive field of 100 Oe and remnant magnetization of 0.012 emu g⁻¹ for sample No. 2 was obtained. The results of the VSM study demonstrated dual magnetic behavior, ferromagnetic nature in low field and paramagnetic nature in up field, of the (Co, Mn)(Co, Mn)₂O₄ nanoparticles.

3.5. Optical features

Understanding the optical properties of nanoparticles is an essential component when examining their photocatalytic activity. A complete

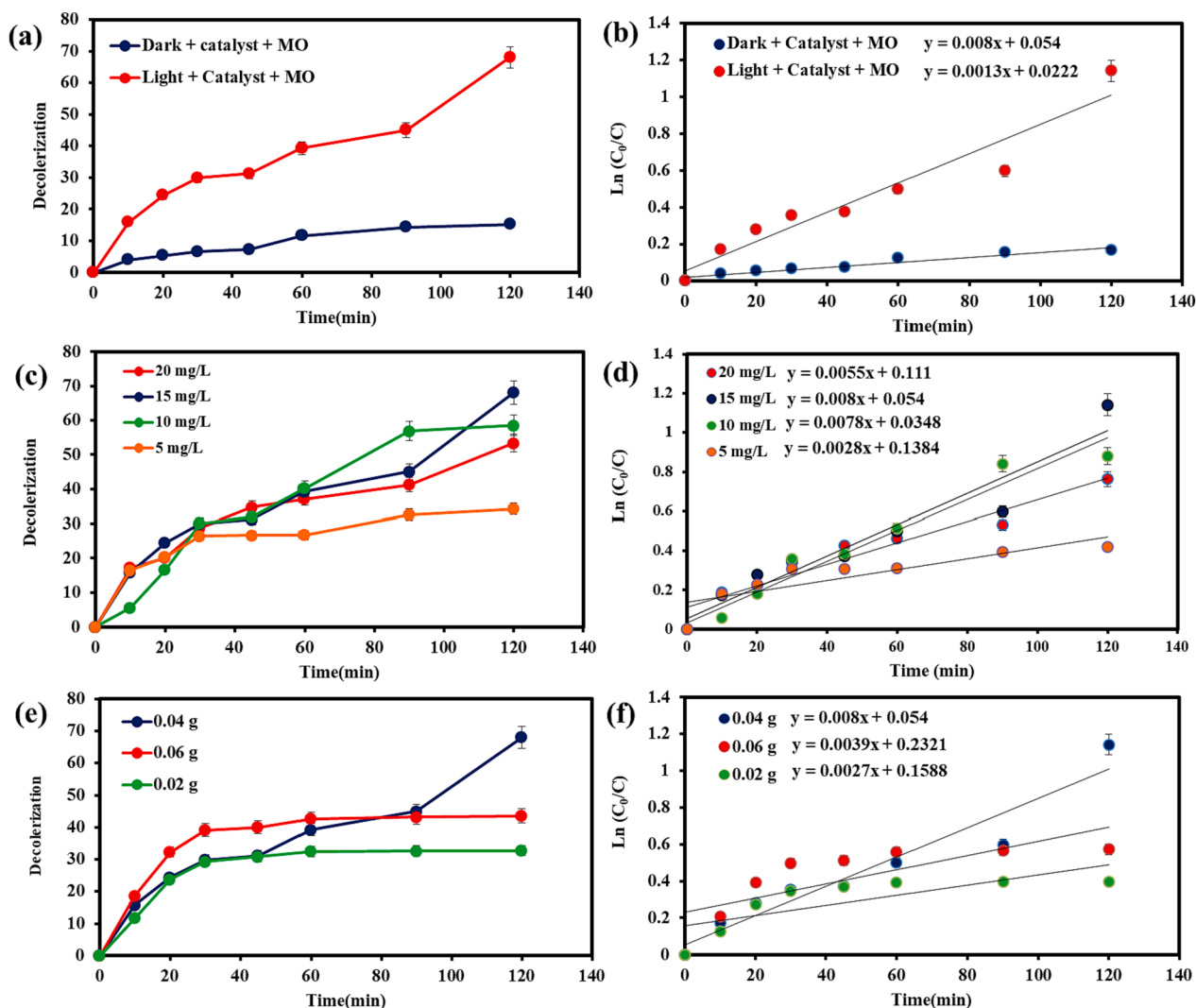


Fig. 5. Photocatalytic activities and kinetic linear simulation plots of the (Co, Mn)(Co, Mn)₂O₄ nanoparticles (a, b) Investigating the MO removal in the dark and visible light after 120 min, (c, d) Investigating the effect of different concentrations of MO, and (e, f) Investigating the effect of different amounts of catalyst on the photocatalysis process under visible radiation.

survey of the optical properties of the (Co, Mn)(Co, Mn)₂O₄ nanoparticles (sample No. 2) was conducted through the utilization of DRS analysis and the relative results is illustrated in Figure S3. The absorption spectrum of optimized product depicts a light absorption edge in wider range from 200 to 700 nm. By using the Tauc's equation (Tauc et al., 1966), the estimated band-gap for these nanoparticles was calculated to be about 1.7 eV which is showed in inset of Figure S3. In light of the above analysis, it recommended that the synthesized (Co, Mn)(Co, Mn)₂O₄ nanoparticles can be introduced as an effective and promising catalyst in the advanced photocatalysis applications.

3.6. Photoactivity of catalyst

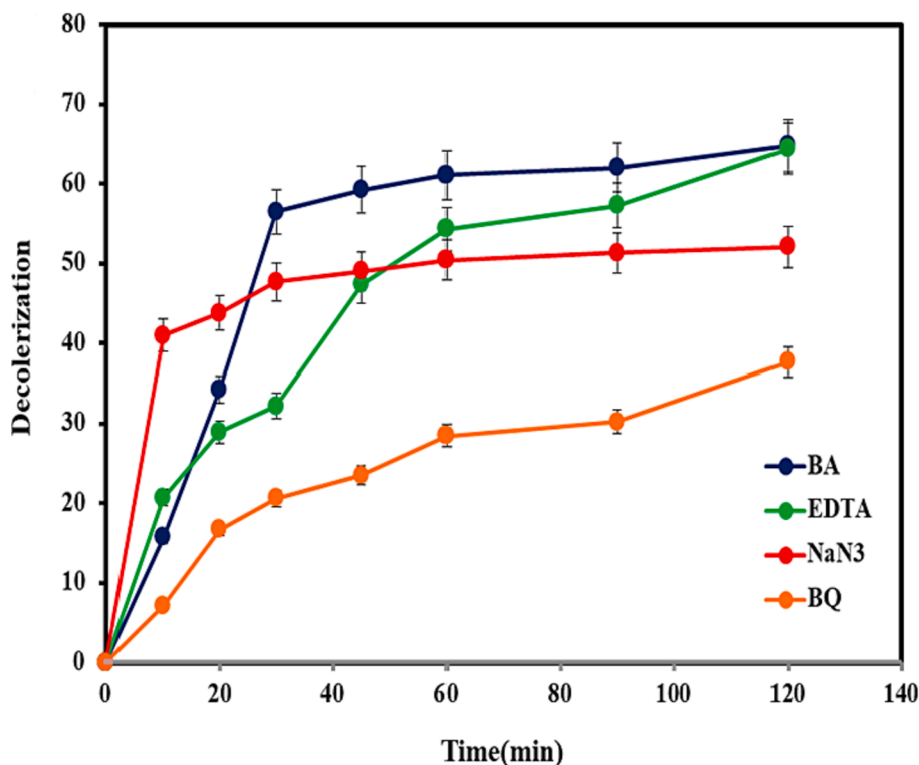
Thoroughly researching the photocatalysis process necessitates carrying out several steps, such as assessing the effect of dye adsorption on the catalyst, the impact of pH and temperature, the impact of the photocatalyst, and so on (Boruah et al., 2019; Jamdar et al., 2024). Generally, to elucidate the photodegradation mechanism of a semiconductor, possibility of three ways such as (i) photolysis, (ii) dye photosensitization, and (iii) photocatalysis are examined (Jiang et al., 2015) (Scheme 2). It can be found that the negatively charged electron on the excited dye molecules is trapped by the oxygen molecules to create a singlet oxygen atom, which has strong oxidation capability to photolysis pure dye. An initial experiment was conducted to assess the effect of visible light on the discoloration of MO for 120 min at room

temperature in order to evaluate the effect of light itself, namely photolysis. In this process, the dye was slightly degraded under visible (6.0 %) light. On the other hand, the organic dye photosensitization activity involves the structural stability of dye molecules during indirect process of degradation (Yu, C. et al., 2013), in which the adsorbed MO are stimulated to produce photoinduced electrons under energy of the irradiating light and then transfer them to the conduction band of the semiconductor, resulting in further oxidative transformations. Afterwards, the experiment was carried out in the dark to evaluate the adsorption of the dye onto the catalysts. The purpose of this process was to measure the amount of dye that was adsorbed onto (Co, Mn)(Co, Mn)₂O₄ nanoparticles. Fig. 5a describes the decolorization performances of MO solution with (Co, Mn)(Co, Mn)₂O₄ nano-catalyst under dark and visible light illumination. In the dark, the MO adsorption rate over synthesized (Co, Mn)(Co, Mn)₂O₄ nanoparticles showed the percentage of 15.28 % after 120 min. It is clear that the possibility of both process namely, photolysis and dye photosensitization in MO decomposition cannot be ignored. Subsequently, photocatalysis was implemented to eliminate MO from the aqueous solution under visible lights. As seen from the Fig. 5a, discoloration under light source showed a higher removal percentage (68.07 %). In the following, four different concentrations of MO (5, 10, 15, and 20 mg/L) were investigated under visible light in the photocatalysis process. The designed model for the

Table 2

Comparison of photodegradation performance of our fabricated samples with earlier reports.

Photocatalyst	Method	Targeted Pollutants	Light source	Contact time	Percentage%	Ref.
Cu-MnO ₂	Chemical synthesis	Brilliant Green	visible light	180 min	73.1 %	(Mondal et al., 2019)
CoMn ₂ O ₄	Co-precipitation	Congo Red	Direct sunlight	120 min	52.78 %	(Mark et al., 2021)
Co ₃ O ₄	Co-precipitation	Methyl orange	visible light	120 min	64.4 %	(Zeid et al., 2023)
MnO ₂	Wet-chemical	Tetracycline	Visible light	60 min	36.41 %	(Du et al., 2021)
CoMoO ₄	Refluxing	Rhodamine B	Visible light	300 min	37.4 %	(Pirhashemi and Habibi-Yangjeh, 2018)
Mn _{0.2} Co _{0.8} Zr _{0.15} Fe _{1.85} O ₄	Co-precipitation	Alizarin Yellow R	Visible light	120 min	52.45 %	(Ahmed et al., 2021)
(Co, Mn)(Co, Mn) ₂ O ₄	Combustion	Methyl orange	Visible light	120 min	68.07 %	This work

Fig. 6. Photocatalytic activity of the (Co, Mn)(Co, Mn)₂O₄ nanoparticles (sample No. 2) in the presence of scavengers.

pollutant's concentration showed an effective role on the photodegradation yield. As it is clear in Fig. 5c, the photodegradation efficiencies of dye solution within 120 min of visible light irradiation were found to be 34.21 %, 58.52 %, 68.07 %, and 53.35 %, corresponding to 5, 10, 15, and 20 mg/L of pollutant, respectively. The highest discoloration percentage was achieved at the concentration of 15 mg/L. This findings exhibits that the saturation of the (Co, Mn)(Co, Mn)₂O₄ surface with excessive dye molecules can be the fact for low photocatalytic decolorization. However, when the initial contaminant concentration was less than the certain amount (5 and 10 mg/L), high relative number of reactive sites on the surface of the (Co, Mn)(Co, Mn)₂O₄ could provide the rapid degradation of MO (Cui et al., 2021). After employing the optimized concentration of contaminant solution, three different amounts of photocatalyst (0.02, 0.04, and 0.06 g) were used to check the effect of the catalyst loading on discoloration. As shown in Fig. 5e, while increasing the dosage of the (Co, Mn)(Co, Mn)₂O₄ nanophotocatalysts from 0.02 to 0.04 g, the change in photodegradation efficiency could show an increase rate from 32.77 % to 68.07 %, but precautions are needed. This enhancement is due to the combined effect of higher surface area and more active site of synthesized catalyst, which can easily absorb photons to promote the final efficiency (Cui et al., 2021). When the (Co, Mn)(Co, Mn)₂O₄ dosage exceeded the amount of 0.04 g, the removal rate of MO started to decline (43.57 %). In this case, reducing the penetration of light and light scattering may be reason for the

limitation of the concentration of photo-generated carriers (Panahi et al., 2023a). To further elucidate the photocatalytic degradation kinetics of the resultant samples, the Langmuir-Hinshelwood first-order reaction kinetics model was adapted under a variety of photocatalytic reaction conditions, which is described below (Shanmugam et al., 2023):

$$\ln(C_0/C) = kt \quad (4)$$

Where C_0 and C represent initial and final MO concentration in the solution at an initial irradiation time of $t = 0$ and at time of t , respectively, whereas k expresses the degradation rate constant. From the logarithmic analysis of the absorbance content vs the irradiation time (Fig. 5(b, d, f)), it can be observed that the maximum linear fitted value in the form of straight line confirm superior photocatalytic efficiency (0.008 min^{-1}) for (Co, Mn)(Co, Mn)₂O₄ nanostructures at 15 mg/L of MO molecules with 0.04 g of catalyst. In Table 2, the comparison of photoactivity conditions of the as-obtained (Co, Mn)(Co, Mn)₂O₄ nanoparticle with previously reported papers has been summarized.

To further distinguish the role of active free radicals in the photodegradation rate, the relative mechanism was analyzed via the trapping experiments of radicals. Different compounds are employed to ensnare free radicals (Munawar et al., 2020; Schneider et al., 2020). In this content, BQ, EDTA, BA, and NaN₃ were used to remove superoxide ($\bullet\text{O}_2^-$) radicals, holes (h^+), hydroxyl ($\bullet\text{OH}$) radicals and singlet oxygen

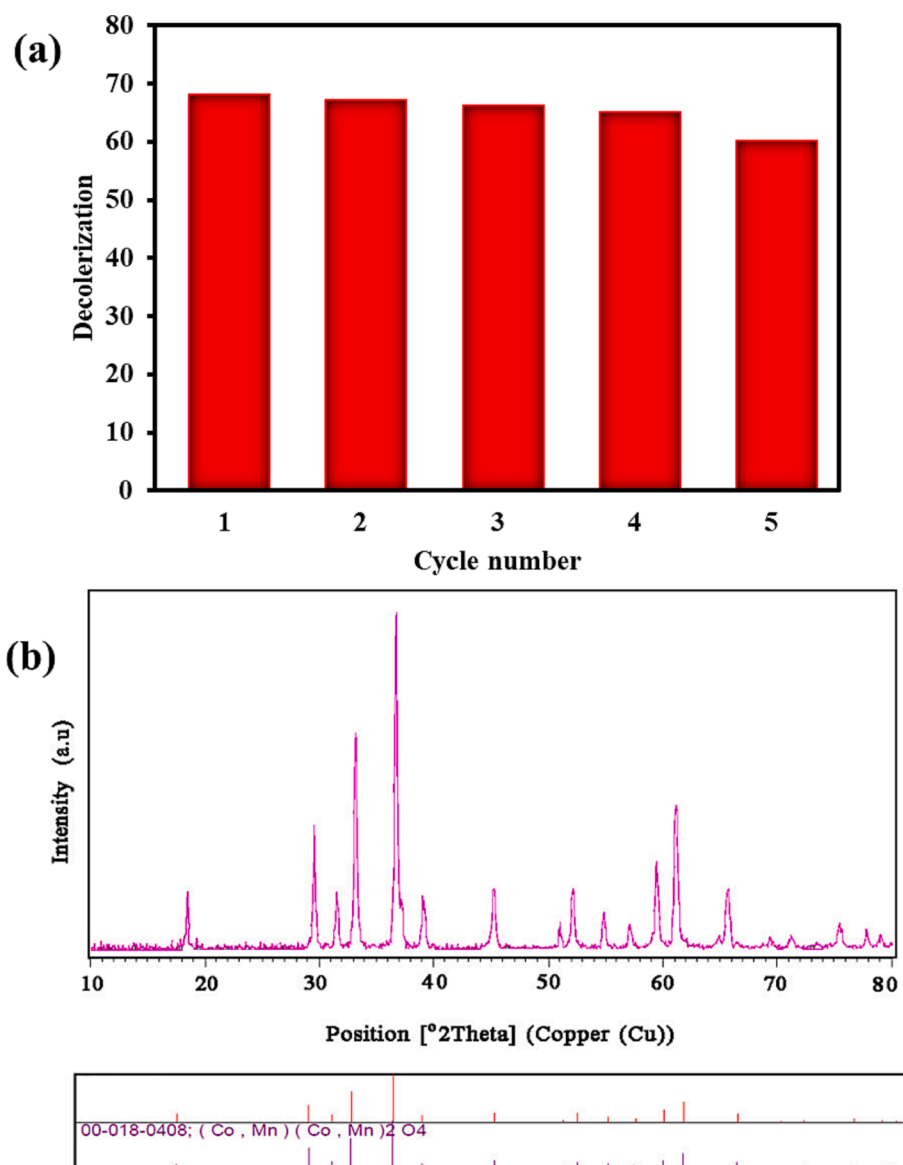
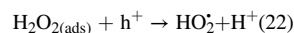
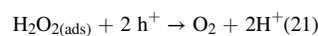
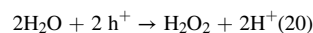
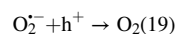
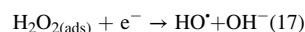
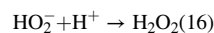
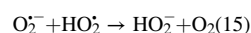
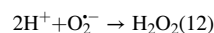
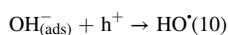
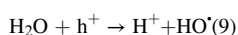
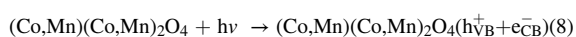
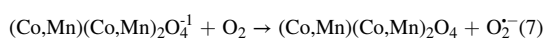
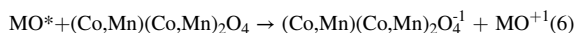
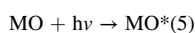


Fig. 7. (a) Recycle efficiency and (b) XRD pattern of the (Co, Mn)(Co, Mn)₂O₄ after five cycles of photocatalytic reaction.

(¹O₂), respectively. As shown in Fig. 6, the photocatalytic activity of the (Co, Mn)(Co, Mn)₂O₄ nanoparticles is decreased significantly in the presence of BQ. In addition, NaN₃ also decreased the discoloration rate, but not intensively. Therefore, it can be concluded that $\bullet\text{O}_2^-$ and ¹O₂ species have more important role in the photocatalytic discoloration of MO by using (Co, Mn)(Co, Mn)₂O₄ nanoparticles under visible radiation. The possible photocatalytic mechanism for removal of MO dye by Co–Mn–O nanostructures can be summarized as (Karami et al., 2022; Panahi et al., 2023b):



MO + OH[•] → Degradation products (e.g., CO₂, H₂O, H₂) (24)

MO + h⁺_{VB} → Oxidation products (25)

MO + e⁻_{CB} → Reduction products (26)

Fig. 7(a, b) illustrates the photo-stability and reusing of as-formed (Co, Mn)(Co, Mn)₂O₄ nanoparticles under visible light. After recycling process, Co-Mn-O powders were centrifuged, washed with distilled water, and then dried at 60 °C for 20 h. After that, the second run of photoactivity test was accomplished in the presence of previously used (Co, Mn)(Co, Mn)₂O₄ structures and fresh MO solution. As illustrated in Fig. 7a, the removal efficiency expresses 60.1 % after five repetitions of photodegradation performance. The XRD pattern of the reused (Co, Mn)(Co, Mn)₂O₄ nano-catalysts was carried out to test the impacts of light and high temperatures during drying on structural degradation. The diffraction peaks of sample in Fig. 7b confirm that the host composition is related to (Co, Mn)(Co, Mn)₂O₄ (JCPDS No. 00–018-0408, tetragonal structure).

4. Conclusion

To conclude, the employing glycine as both fuel and capping agent in facile auto-combustion method enabled the successful synthesis of the (Co, Mn)(Co, Mn)₂O₄-based compounds. Several synthesis conditions, including modifications in the proportion of ingredients (Co:Mn) and the addition of glycine, were employed to create particles with desired size and shape. In accordance with XRD and FESEM analyses, the sample prepared with a ratio of 1 to 3 of Co:Mn precursors with no impurity was selected as the optimal sample (Sample No.2). Optical band gap of tetragonal (Co, Mn)(Co, Mn)₂O₄ phase was found to be 1.7 eV, which is suitable for visible-light-driven degradation of MO as pollutant model. The dye concentration and the amount of catalyst were examined in order to perform the photocatalysis test in the most optimal way. The photocatalysis test at a dye concentration of 15 mg/L in the presence of 0.04 g of the catalyst with 68.07 % discoloration was the best result after 120 min. Based on the kinetic model, the highest-fitted reaction rate constant was calculated to be 0.008 min⁻¹. An investigation of the photocatalysis process was done with the utilization of scavengers during the photocatalysis test. The results showed that [•]O₂⁻ and ¹O₂ species have important role in the discoloration of MO by using (Co, Mn)(Co, Mn)₂O₄ nanoparticles under visible radiation. The MO photodegradation yield of the host Co-Mn-O nanostructures depicted an imperceptible reduction (~7.97 %) following the five successive cycles under visible region, suggesting broad potential possibilities of mixed spinel structure (Co,Mn)(Co,Mn)₂O₄ nanomaterial for environmental remediation applications. That is to say, these compounds have propitious ability to keep their catalytic activity as well as structural stability. Research on new methods and nanomaterials for the elimination of water impurities will be pursued.

CRedit authorship contribution statement

Ghazal Oroumi: Software, Investigation, Methodology, Formal analysis. **Foroozan Samimi:** Formal analysis, Data curation, Software. **Makarim A. Mahdi:** Writing – review & editing, Software, Data curation, Validation. **Elmuez A. Dawi:** Writing – review & editing, Software, Conceptualization. **Masoud Salavati-Niasari:** Software, Formal analysis, Methodology, Writing – review & editing, Writing – original draft, Conceptualization, Supervision, Project administration, Investigation, Data curation, Validation, Resources, Visualization, Funding acquisition.

Declaration of competing interest

The authors declare that they have no known competing financial interests or personal relationships that could have appeared to influence the work reported in this paper.

Acknowledgements

Authors are grateful to the council of Iran National Science Foundation (97017837) and University of Kashan for supporting this work by Grant No. (159271/GO1).

Appendix A. Supplementary material

Supplementary data to this article can be found online at <https://doi.org/10.1016/j.arabjc.2023.105588>.

References

- Ahmad, N.N.R., Ang, W.L., Teow, Y.H., Mohammad, A.W., Hilal, N., 2022. Nanofiltration membrane processes for water recycling, reuse and product recovery within various industries: A review. *J. Water Process Eng.* 45, 102478.
- Ahmed, A., Usman, M., Wang, S., Yu, B., Shen, Y., Cong, H., 2021. Facile synthesis of Zr4 + substituted MnO₂·2CoO₈Fe₂·xO₄ nanoparticles and their composites with reduced graphene oxide for enhanced photocatalytic performance under visible light irradiation. *Synth. Met.* 277, 116766.
- Aseel M. Aljeboree, R. A. Mohammed, M. Mahdi, Layth S. Jasim, A. Alkaim, Synthesis, Characterization of P(CH/AA-co-AM) and Adsorptive Removal of Pb (II) ions from Aqueous Solution: Thermodynamic Study. *NeuroQuantology* 19(7) (2021) 137-143. 10.14704/nq.2021.19.7.NQ21096.
- Al-Mamun, M., Kader, S., Islam, M., Khan, M., 2019. Photocatalytic activity improvement and application of UV-TiO₂ photocatalysis in textile wastewater treatment: A review. *J. Environ. Chem. Eng.* 7 (5), 103248.
- Amin Marsooli, M., Rahimi Nasrabadi, M., Fasihi-Ramandi, M., Adib, K., Pourmasoud, S., Ahmadi, F., Eghbali, M., Sobhani Nasab, A., Tomczykowa, M., Plonska-Brzezinska, M.E., 2020. Synthesis of magnetic Fe₃O₄/ZnWO₄ and Fe₃O₄/ZnWO₄/CeVO₄ nanoparticles: the photocatalytic effects on organic pollutants upon irradiation with UV-Vis light. *Catalysts* 10 (5), 494.
- Aragaw, T.A., Bogale, F.M., Aragaw, B.A., 2021. Iron-based nanoparticles in wastewater treatment: A review on synthesis methods, applications, and removal mechanisms. *J. Saudi Chem. Soc.* 25 (8), 101280.
- Aslam, I., Farooq, M.H., Ghani, U., Rizwan, M., Nabi, G., Shahzad, W., Boddula, R., 2019a. Synthesis of novel g-C₃N₄ microrods: A metal-free visible-light-driven photocatalyst. *Mater. Sci. Energy Technol.* 2 (3), 401–407.
- Aslam, I., Farooq, M.H., Iqbal, M., Boddula, R., Abid, M., Ashfaq, M., Ghani, U., 2019b. Synthesis of WO₃·H₂O spherical particles for efficient photocatalytic properties under visible light source. *Mater. Sci. Energy Technol.* 2 (2), 187–193.
- Badvi, K., Javanbakht, V., 2021. Enhanced photocatalytic degradation of dye contaminants with TiO₂ immobilized on ZSM-5 zeolite modified with nickel nanoparticles. *J. Clean. Prod.* 280, 124518.
- Behvandi, S., Sobhani-Nasab, A., Karimi, M.A., Sohoul, E., Karimi, M., Ganjali, M.R., Ahmadi, F., Rahimi-Nasrabadi, M., 2020. Synthesis and characterization of Sm₂(MoO₄)₃, Sm₂(MoO₄)₃/GO and Sm₂(MoO₄)₃/C₃N₄ nanostructures for improved photocatalytic performance and their anti-cancer the MCF-7 cells. *Polyhedron* 180, 114424.
- Blaise, A., Barrese, E., Apollaro, C., Miriello, D., 2009. Flux growth and characterization of Ti- and Ni-doped forsterite single crystals. *Crystal Research and Technology: J. Exp. Ind. Crystallogr.* 44 (5), 463–468.
- Bonthula, S., Bonthula, S.R., Pothu, R., Srivastava, R.K., Boddula, R., Radwan, A.B., Al-Qahtani, N., 2023. Recent Advances in Copper-Based Materials for Sustainable Environmental Applications. *Sustain. Chem.* 4 (3), 246–271.
- Boruah, B., Gupta, R., Modak, J.M., Madras, G., 2019. Enhanced photocatalysis and bacterial inhibition in Nb₂O₅ via versatile doping with metals (Sr, Y, Zr, and Ag): a critical assessment. *Nanoscale Adv.* 1 (7), 2748–2760.
- Cui, H., Dong, S., Wang, K., Luan, M., Huang, T., 2021. Synthesis of a novel Type-II In₂S₃/Bi₂MoO₆ heterojunction photocatalyst: Excellent photocatalytic performance and degradation mechanism for Rhodamine B. *Sep. Purif. Technol.* 255, 117758.
- Du, C., Zhang, Z., Tan, S., Yu, G., Chen, H., Zhou, L., Yu, L., Su, Y., Zhang, Y., Deng, F., 2021. Construction of Z-scheme g-C₃N₄/MnO₂/GO ternary photocatalyst with enhanced photodegradation ability of tetracycline hydrochloride under visible light radiation. *Environ. Res.* 200, 111427.
- Ganduh, S.H., Kmal, R.Q., Mahdi, M.A., Aljeboree, A.M., Jasim, L.S., 2021. Selective spectrophotometric determination of 4-amino antipyrine antibiotics in pure forms and their pharmaceutical formulations. *International Journal of Drug Delivery Technology* 11 (2), 371–375.
- Hasan, H.A., Muhammad, M.H., 2020. A review of biological drinking water treatment technologies for contaminants removal from polluted water resources. *J. Water Process Eng.* 33, 101035.

- Holzwarth, U., Gibson, N., 2011. The Scherrer equation versus the 'Debye-Scherrer equation'. *Nat. Nanotechnol.* 6(9), 534-534.
- Hosny, N.M., Gomaa, I., Elmahgary, M.G., 2023. Adsorption of polluted dyes from water by transition metal oxides: A review. *Appl. Surf. Sci. Adv.* 15, 100395.
- Jabbar, Z.H., Graimed, B.H., 2022. Recent developments in industrial organic degradation via semiconductor heterojunctions and the parameters affecting the photocatalytic process: A review study. *J. Water Process Eng.* 47, 102671.
- Jamdar, M., Monsef, R., Ganduh, S.H., Dawi, E.A., Jasim, L.S., Salavati-Niasari, M., 2024. Unraveling the potential of sonochemically achieved DyMnO₃/Dy₂O₃ nanocomposites as highly efficient visible-light-driven photocatalysts in decolorization of organic contamination. *Ecotoxicol. Environ. Saf.* 269, 115801.
- Jiang, Y.-R., Lin, H.-P., Chung, W.-H., Dai, Y.-M., Lin, W.-Y., Chen, C.-C., 2015. Controlled hydrothermal synthesis of BiOxCl_y/BiO_mIn composites exhibiting visible-light photocatalytic degradation of crystal violet. *J. Hazard. Mater.* 283, 787-805.
- Joseph, L., Jun, B.-M., Flora, J.R., Park, C.M., Yoon, Y., 2019. Removal of heavy metals from water sources in the developing world using low-cost materials: A review. *Chemosphere* 229, 142-159.
- Karami, A., Monsef, R., Shihan, M.R., Qassem, L.Y., Falah, M.W., Salavati-Niasari, M., 2022. UV-light-induced photocatalytic response of Pechini sol-gel synthesized erbium vanadate nanostructures toward degradation of colored pollutants. *Environ. Technol. Innov.* 28, 102947.
- Karthikeyan, C., Arunachalam, P., Ramachandran, K., Al-Mayouf, A.M., Karuppuchamy, S., 2020. Recent advances in semiconductor metal oxides with enhanced methods for solar photocatalytic applications. *J. Alloys Compd.* 828, 154281.
- Kihal, I., Douafer, S., Lahmar, H., Rekhila, G., Hcini, S., Trari, M., Benamira, M., 2024. CoMn₂O₄: A new spinel photocatalyst for hydrogen photo-generation under visible light irradiation. *J. Photochem. Photobiol. a: Chem.* 446, 115170.
- Liang, Q., Chen, K., Hou, W., Yan, Q., 1998. CO hydrogenation over nanometer spinel-type Co/Mn complex oxides prepared by sol-gel method. *Appl. Catal. a: Gen.* 166 (1), 191-199.
- Lin, J., Zeng, C., Xu, J., Zeb, A., Lin, X., Hu, L., Li, K., Xu, X., 2021. Oxygen vacancy engineering of carbon-encapsulated (Co, Mn)₂(Co, Mn)O₄ from metal-organic framework towards boosted lithium storage. *Chem. Eng. J.* 425, 130661.
- Lu, Q., Wei, Z., Ding, M., Li, C., Ma, J., 2023. Properties of g-C₃N₄ modified mixed spinel structure (Co, Mn)₂(Co, Mn)O₄ cathode material for supercapacitor. *J. Solid State Chem.* 322, 123973.
- Makarim A. Mahdi, Aseel M. Aljeboree, Layth S. Jasim, Ayad F. Alkaim, Synthesis, Characterization and Adsorption Studies of a Graphene Oxide/Polyacrylic Acid Nanocomposite Hydrogel. *NeuroQuantology*, 19 (9) (2021) 46-54. 10.14704/nq.2021.19.9.NQ21136.
- Mark, J.A.M., Venkatachalam, A., Pramothkumar, A., Senthilkumar, N., Jothivenkatachalam, K., prince Jesuraj, J., 2021. Investigation on structural, optical and photocatalytic activity of CoMn₂O₄ nanoparticles prepared via simple co-precipitation method. *Phys. B: Condens. Matter.* 601, 412349.
- Marsooli, M.A., Rahimi-Nasrabadi, M., Fasihi-Ramandi, M., Adib, K., Eghbali-Arani, M., Ahmadi, F., Sohoul, E., Sobhani nasab, A., Mirhosseini, S.A., Gangali, M.R., 2020. Preparation of Fe₃O₄/SiO₂/TiO₂/CeVO₄ nanocomposites: investigation of photocatalytic effects on organic pollutants, bacterial environments, and new potential therapeutic candidate against cancer cells. *Front. Pharmacol.* 11, 192.
- Masi, A., Bellusci, M., Carlini, M., McPhail, S.J., Padella, F., Reale, P., 2016. Mechanochemical processing of Mn and Co oxides: an alternative way to synthesize mixed spinels for protective coating. *J. Am. Ceram. Soc.* 99 (1), 308-314.
- Mkhalid, I.A., Ismail, A.A., Hussein, M.A., Al Thomali, R.H., 2023. Nanoheterojunctions MnCo₂O₄ nanoparticles anchored on mesoporous TiO₂ networks for superior photocatalytic ability. *Mater. Res. Bull.* 167, 112439.
- Mondal, D., Das, S., Paul, B.K., Bhattacharya, D., Ghoshal, D., Gayen, A.L., Das, K., Das, S., 2019. Size engineered Cu-doped α-MnO₂ nanoparticles for exaggerated photocatalytic activity and energy storage application. *Mater. Res. Bull.* 115, 159-169.
- Monsef, R., Salavati-Niasari, M., 2023. Fundamental understanding on cyclability behaviors of ammonium vanadate nanoarchitectures as cathode materials for Li-ion batteries: A comparative insight of dual modification of precursor and morphology. *J. Energy Storage* 74, 109395.
- Munawar, T., Yasmeen, S., Hasan, M., Mahmood, K., Hussain, A., Ali, A., Arshad, M., Iqbal, F., 2020. Novel tri-phase heterostructured ZnO-Yb₂O₃-Pr₂O₃ nanocomposite; structural, optical, photocatalytic and antibacterial studies. *Ceram. Int.* 46 (8), 11101-11114.
- Naik, R., Revathi, V., Murthy, H.A., Nagaswarupa, H., Ravikumar, C., Reddy, G.A., Pothu, R., Boddula, R., Lokesh, H., Shanbhag, V., 2023. Multifunctional La₁₀Si₆O₂₇: Tb³⁺ tailored material for photoluminescence, photocatalysis and electrochemical sensing applications. *Appl. Surf. Sci. Adv.* 14, 100392.
- Obotey Ezugbe, E., Rathilal, S., 2020. Membrane technologies in wastewater treatment: a review. *Membranes* 10 (5), 89.
- Onwudiwe, D.C., Olatunde, O.C., Nkwe, V.M., Smida, Y.B., Ferjani, H., 2023. Dual S-scheme heterojunction g-C₃N₄/Bi₂S₃/CuS composite with enhanced photocatalytic activity for methyl orange degradation. *Inorg. Chem. Commun.* 155, 111075.
- Panahi, A., Ghanbari, M., Dawi, E.A., Monsef, R., Abass, R.R., Aljeboree, A.M., Salavati-Niasari, M., 2023a. Simple sonochemical synthesis, characterization of TmVO₄ nanostructure in the presence of Schiff-base ligands and investigation of its potential in the removal of toxic dyes. *Ultrason. Sonochem.* 95, 106362.
- Panahi, A., Monsef, R., Imran, M.K., Mahdi, A.A., Ruhaima, A.A.K., Salavati-Niasari, M., 2023b. TmVO₄/Fe₂O₃ nanocomposites: Sonochemical synthesis, characterization, and investigation of photocatalytic activity. *Int. J. Hydrog. Energy* 48 (10), 3916-3930.
- Pirhashemi, M., Habibi-Yangjeh, A., 2018. Facile fabrication of novel ZnO/CoMoO₄ nanocomposites: Highly efficient visible-light-responsive photocatalysts in degradations of different contaminants. *J. Photochem. Photobiol. a: Chem.* 363, 31-43.
- Rahimi-Nasrabadi, M., Ghaderi, A., Banafshe, H.R., Eghbali-Arani, M., Akbari, M., Ahmadi, F., Pourmasoud, S., Sobhani-Nasab, A., 2019. Preparation of Co₂TiO₄/CoTiO₃/Polyaniline ternary nano-hybrids for enhanced destruction of agriculture poison and organic dyes under visible-light irradiation. *J. Mater. Sci. Mater. Electron.* 30, 15854-15868.
- Ren, G., Han, H., Wang, Y., Liu, S., Zhao, J., Meng, X., Li, Z., 2021. Recent advances of photocatalytic application in water treatment: A review. *Nanomaterials* 11 (7), 1804.
- Rostami, M., Sharafi, P., Mozaffari, S., Adib, K., Sobhani-Nasab, A., Rahimi-Nasrabadi, M., Fasihi-Ramandi, M., Ganjali, M.R., Badii, A., 2021. A facile preparation of ZnFe₂O₄-CuO-N/B/RGO and ZnFe₂O₄-CuO-C₃N₄ ternary heterojunction nanophotocatalyst: characterization, biocompatibility, photo-Fenton-like degradation of MO and magnetic properties. *J. Mater. Sci. Mater. Electron.* 32, 5457-5472.
- Schneider, J.T., Firak, D.S., Ribeiro, R.R., Peralta-Zamora, P., 2020. Use of scavenger agents in heterogeneous photocatalysis: truths, half-truths, and misinterpretations. *Phys. Chem. Chem. Phys.* 22 (27), 15723-15733.
- Shanmugam, P., Rajakumar, K., Boddula, R., Ngullie, R.C., Wei, W., Xie, J., Murugan, E., 2019. Heterogeneous form of poly (4-vinyl pyridine) beads based dendrimer stabilized Ag, Au and PdNPs catalyst for reduction of trypan blue. *Mater. Sci. Energy Technol.* 2 (3), 532-542.
- Shanmugam, P., Ngullie, R.C., Smith, S.M., Boonyuen, S., Boddula, R., Pothu, R., 2023. Visible-light induced photocatalytic removal of methylene blue dye by copper oxide decorated zinc oxide nanorods. *Mater. Sci. Energy Technol.* 6, 359-367.
- Taghipour, S., Hosseini, S.M., Ataie-Ashtiani, B., 2019. Engineering nanomaterials for water and wastewater treatment: review of classifications, properties and applications. *New J. Chem.* 43 (21), 7902-7927.
- Taifi A., Alkadir O. K. A., Oda A. A., Aljeboree A. M., Al Bayaa A. L., Alkaim A. F., Abed S. A. "Biosorption by Environmental, Natural and Acid-Activated Orange Peels as Low-Cost Adsorbent: Optimization of Disperse Blue 183 as a Model";(2022) IOP Conference Series: Earth and Environmental Science, 1029 (1), art. no. 012009. DOI: 10.1088/1755-1315/1029/1/012009.
- Tang, W., Ren, Z., Lu, X., Wang, S., Guo, Y., Hoang, S., Du, S., Gao, P.X., 2017. Scalable integration of highly uniform Mn_xCo_{3-x}O₄ nanosheet array onto ceramic monolithic substrates for low-temperature propane oxidation. *ChemCatChem* 9 (21), 4112-4119.
- Tauc, J., Grigorovici, R., Vancu, A., 1966. Optical properties and electronic structure of amorphous germanium. *Phys. Status Solidi B* 15 (2), 627-637.
- Topka, P., Jirátořová, K., Dvořáková, M., Balabánová, J., Kostejn, M., Kovanda, F., 2021. Hydrothermal deposition as a novel method for the preparation of Co-Mn mixed oxide catalysts supported on stainless steel meshes: application to VOC oxidation. *Environ. Sci. Pollut. Res.* 1-12.
- Wang, W., Xu, M., Xu, X., Zhou, W., Shao, Z., 2020. Perovskite oxide based electrodes for high-performance photoelectrochemical water splitting. *Angew. Chem. Int. Ed.* 59 (1), 136-152.
- Yaqoob, A.A., Parveen, T., Umar, K., Ibrahim, M., Nasir, M., 2020. Role of nanomaterials in the treatment of wastewater: a review. *Water* 12 (2), 495.
- Yu, C., Li, G., Kumar, S., Kawasaki, H., Jin, R., 2013a. Stable Au₂₅(SR)₁₈/TiO₂ composite nanostructure with enhanced visible light photocatalytic activity. *J. Phys. Chem. Lett.* 4 (17), 2847-2852.
- Yu, L., Zhang, L., Wu, H.B., Zhang, G., Lou, X.W.D., 2013b. Controlled synthesis of hierarchical Co_xMn_{3-x}O₄ array micro-/nanostructures with tunable morphology and composition as integrated electrodes for lithium-ion batteries. *Energy Environ. Sci.* 6 (9), 2664-2671.
- Zeid, E.F.A., Obiedallah, F.M., Abu-Sehly, A.-H., Mohamed, W.A., Abd El-Aal, M., 2023. A comparative study of single and bi-doped Co₃O₄ nanocatalysts for the photodegradation of methyl orange dye. *J. Mol. Struct.* 1293, 136203.
- Zhao, A., Masa, J., Xia, W., Maljusch, A., Willinger, M.-G., Clavel, G., Xie, K., Schlögl, R., Schuhmann, W., Muhler, M., 2014. Spinel Mn-Co oxide in N-doped carbon nanotubes as a bifunctional electrocatalyst synthesized by oxidative cutting. *J. Am. Chem. Soc.* 136 (21), 7551-7554.